GEOLOGICAL EVOLUTION OF THE MAFIC AND FELSIC GRANULITES FROM THE CENTRAL AND NORTHWESTERN PARTS OF THE EASTERN GHATS PROVINCE IN THE CONTEXT OF GRENVILLIAN-AGE TECTONICS

Thesis submitted for the partial fulfillment of the requirements for the degree Doctor of Philosophy in Science

by

Arnob Kumar Mondal

Under the supervision of

Prof. Sankar Bose

and

Prof. Gautam Ghosh

Department of Geology

Faculty of Natural and Mathematical Sciences

Presidency University

Kolkata, India

2023

Thesis Title: GEOLOGICAL EVOLUTION OF THE MAFIC AND FELSIC GRANULITES FROM THE CENTRAL AND NORTHWESTERN PARTS OF THE EASTERN GHATS PROVINCE IN THE CONTEXT OF GRENVILLIAN-AGE TECTONICS

Name of the Candidate: Arnob Kumar Mondal

Registration Number: R-19RS215170198

Date of Registration: 6th January, 2021

Department: Geology

Arnob Kumar Mondal
21/11/2023

Signature of the candidate with date

DECLARATION

I hereby declare that this thesis contains original research work carried out by me under the guidance of Prof. Sankar Bose and Prof. Gautam Ghosh, Professor, Department of Geology, Presidency University, Kolkata, India as part of the PhD programme.

All information in this document have been obtained and presented in accordance with academic rules and ethical conduct.

I also declare that, as required by these rules and conduct, I have fully cited and referenced all materials and results that are not original to this work.

I also declare that, this work has not been submitted for any degree either in part or in full to any other institute or University before.

Arnab Kumar Mandal
21/11/2023
Signature of the candidate with date

This thesis is dedicated to my parents

For their endless support and encouragement

PRESIDENCY UNIVERSITY
KOLKATA

Presidency University

Hindoo College (1817-1855), Presidency College (1855-2010)

CERTIFICATE

This is to certify that the thesis entitled "**GEOLOGICAL EVOLUTION OF THE MAFIC AND FELSIC GRANULITES FROM THE CENTRAL AND NORTHWESTERN PARTS OF THE EASTERN GHATS PROVINCE IN THE CONTEXT OF GRENVILLIAN-AGE TECTONICS**" submitted by Shri/~~Smt~~ **Arnob Kumar Mondal**, Registration Number **R-19RS215170198** and date of registration **6th January, 2021**, in partial fulfilment of the requirements for the award of "**Doctor of Philosophy**", is a record of bonafide research work carried out by him/~~her~~ under ~~my~~/our supervision.

Neither his/~~her~~ thesis nor any part of the thesis has been submitted for any degree/diploma or any other academic award anywhere before.

Signature of the Supervisor(s) with date and official stamp

1_____ 10/11/2023

Dr. Sankar Bose
Professor of Geology
Presidency University
Kolkata - 700 073

2_____ 10/11/2023

GAUTAM GHOSH, PhD
Professor of Geology
Department of Geology
Presidency University, Kolkata, INDIA

86/1, College Street, Kolkata - 700 073, Phone : (033) 2241 1960, Fax : (033) 2241 2738

DrillBit

The Report is Generated by DrillBit Plagiarism Detection Software

Submission Information

Author Name	Arnob Kumar Mondal
Title	GEOLOGICAL EVOLUTION OF THE MAFIC AND FELSIC GR..
Paper/Submission ID	1089985
Submitted by	sankar.geol@presiuniv.ac.in
Submission Date	2023-11-08 12:47:19
Total Pages	89
Document type	Thesis

Result Information

Similarity **8 %**

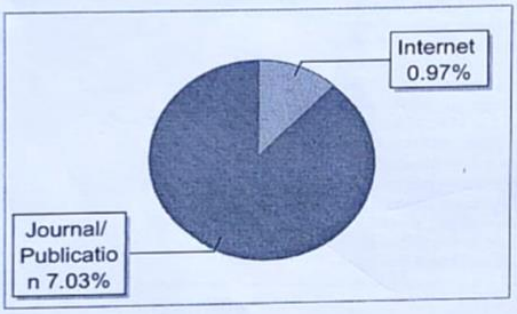

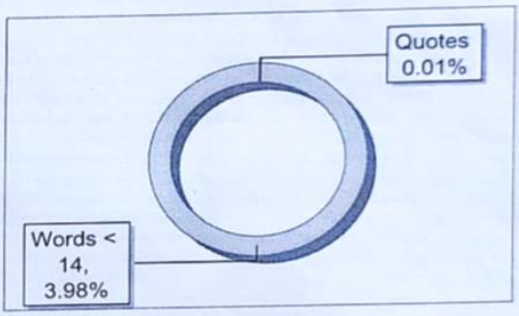

Exclude Information

Quotes	Not Excluded
References/Bibliography	Not Excluded
Sources: Less than 14 Words Similarity	Not Excluded
Excluded Source	**22 %**
Excluded Phrases	Not Excluded

A Unique QR Code use to View/Download/Share Pdf File

Dr. Sankar Bose
Professor of Geology
Presidency University
Kolkata - 700 073

GAUTAM GHOSH, PhD
Professor of Geology
Department of Geology
Presidency University, Kolkata, INDIA

Arnob Kumar Mondal

Head
Department of Geology
Presidency University, Kolkata

ACKNOWLEDGEMENT

I want to express my deep appreciation and heartfelt thanks to my supervisor, Prof. Sankar Bose, for his unwavering support throughout my Ph.D. journey and research endeavours. His patience, encouragement, and extensive expertise have been invaluable. Throughout the research and writing process of this thesis, his guidance proved indispensable. I am also grateful to Prof. Gautam Ghosh for his constant support and guidance during my Ph.D. tenure. I'd like to express my gratitude to the Department of Geology at Presidency University for granting me access to the institutional resources necessary for conducting my research. Special thanks to Mr. Jaganath Pradhan and Mr. Surojit Bag for their support during sample preparation and in other aspects. I wish to express my sincerest gratitude to my collaborators Dr. Nilanjana Sorcar, Dr. Sneha Mukherjee, Amal Deb and Dr. J.K Tomson from NCESS, India for their support during EPMA, XRF and LA-ICPMS analysis. I'd like to convey my deepest appreciation to Dr. Kaushik Das, Associate Professor in the Department of Earth and Planetary System Sciences at Hiroshima University, for his invaluable assistance during the ICP-MS analysis.

I am thankful to all my fellow lab mates from Metamorphic Petrology Lab of Presidency University, with special appreciation for Dr. Proloy Ganguly, Shuvankar Karmakar for their support during field work and creating a suitable work environment in the lab. A special thanks to Shrayasi Das, a dear friend.

I would like to express my gratitude towards CSIR and MoES for the research funding. Last but not least, I would like to thank Gosthipati sir who first taught me how to study thin sections under microscope.

LIST OF ABBREVIATIONS

WDC- Western Dharwar Craton; EDC- Eastern Dharwar Craton; BC-Bastar Craton; SC-Singhbhum Craton; BnC- Bundelkhand Craton; EGB- Eastern Ghats Belt; MB- Mahakoshal Belt; SGT- Southern Granulite Terrain, CGGC- Chotnagpur Granite Gneiss; NSFB- North Singhbhum Fold Belt; CB- Chattisgarh Basin, CuB- Cuddapah Basin, CpG- Cosepect Granite. MSZ- Mahanadi Shear Zone, VSZ- Vamsadhara Shear Zone, NSZ- Nagavalli Shear Zone, SSZ- Sileru Shear Zone, KSZ- Koraput-Sonepur Shear Zone, EBSZ- Eastern Ghats Boundary Shear Zone, KFZ- Kerajung Fault Zone, CGGC: Chotanagpur Gneissic Complex, MR: Mahanadi Rift, GR: Godavari Rift, SGT: Southern Granulite Terrain, WC: Wanni Complex, HC: Highland Complex, VC: Vijayan Complex, KP: Krishna Province, EGP: Eastern Ghats Province, LHC: Lutzow-Holm Complex, NC: Napier Complex, RP: Rayner Province, nPCM: Northern Prince Charles Mountains, FL: Fisher and Lambert terranes, RG: Ruker Group, VH: Vestfold Hills.

LIST OF TABLES

LIST OF FIGURES

Geological Survey of India (2002). (c) Broad geological map of Boudh area northern part of Eastern Ghats Province. (d) Geological map of Bolangir area north-western part of Eastern Ghats Province modified after district resource map by Geological Survey of India (2002).

Figure 5.1-5.12 Photomicrographs and Back- scattered electron (BSE) images of the massif type charnockite. (1) Iron oxide development along the fracture of orthopyroxene (Opx). (2) Spongy intergrowth of garnet and quartz (Qtz) along the margin of orthopyroxene. (3) Thin collar of quartz (Qtz) along the margin of porphyroblastic garnet (Grt_1) grains. (4) A double corona of intergrown garnet and quartz (Grt_2 + Qtz) surrounding porphyroblastic orthopyroxene (Opx) and ilmenite (Ilm). (5) Double corona of quartz (Qtz) and finer matrix garnet (Grt_2) around coarse orthopyroxene (Opx). (6) Porphyroblastic clinopyroxene (Cpx) showing replacement to hornblende (Hbl) and locally biotite (Bt). (7) Partial breakdown of biotite (Bt) to a skeletal intergrowth of K-feldspar and ilmenite (Kfs + Ilm). (8) Antiperthitic texture in plagioclase (Pl), showing irregular blebs and patches of K-feldspar (Kfs). (9) Oval inclusions of quartz (Qtz) and plagioclase (Pl) within coarse perthitic feldspar (Kfs). Note the occurrence of myrmekitic intergrowth along margins of Kfs. (10) Coarse and fine intergrowth of plagioclase (Pl) and quartz (Qtz). (11) Intergrowth of biotite (Bt) and quartz (Qtz) replacing the porphroblastic orthpyroxene (Opx). (12) Cuspate grain boundaries between quartz (Qtz) and plagioclase (Pl) grains.

Figure 5.13-5.28 Multiple plots of geochemical data of the massif type charnockite. (13) Total alkali vs silica (TAS) diagram (after Middlemost, 1994) plot of the samples. The filled circles represent the low-SiO_2 group and the open circles represent the high-SiO_2 group as described in the text. (14) An-Ab-Or triangular plot of the same samples. Fields showing charnockites from the northern Prince Charles Mountains (nPCM), Mawson Coast and Grove Mountains are shown after Sheraton et al. (1996), Zhao et al. (1997), Young et al. (1997), and Liu et al. (2009) are given for comparison. (15) SiO_2–Fe* plot (after Frost and Frost, 2008) of the same samples showing the similarity of the studied samples with the intermediate charnockites described by Rajesh and Santosh (2004). The other fields are same as (14). (16) Y vs. 1000* Ga/Al plot. (17) Modified alkaline-lime index (MALI) plot after Frost et al., (2001) show broad range from calcic to alkali-calcic. (18) A/CNK vs A/NK plot of the same samples. Note that the samples (both high- and low-SiO_2 groups) show metaluminous to weakly peraluminous characters. (19) Th vs Co plot after Hastie et al. (2007). (20) Yb_N vs La_N/Yb_N binary plot of the same samples after Martin (1986). (21) Multi-element variation diagram for trace elements and REE of 14 samples normalized to MORB (after Sun and McDonough, 1989). Note the strong positive anomalies of Th, La, Ce and Nd while strong negative anomalies are found for Nb, P, Sr and Ti. (22) Triangular Rb-Ba-Sr plot. See Rajesh and Santosh (2004) for details on the fields. (23) Sr/Y vs. Y plot, the fields are from Drummond and Defant (1990). (24) Rb vs. Sr plot after Tomson et al., (2006). (25) Th/U vs La/Th plot. Field of common igneous rocks are from Rudnick and Presper (1990). (26) log (Nb/Zr) vs. log Zr plot of the samples (the fields are from Thieblemont and Tegyey, 1994) showing all the samples plotting in the collision field. (27) Nb/La vs La/Yb plot of the same samples after Hollocher et al. (2012). Note the samples plot in the fields of alkaline arc to continental arc. (28) Chondrite-normalized REE plot (after

McDonough and Sun, 1995) of the samples showing strongly fractionated REE patterns with a prominent negative Eu anomaly.

Figure 5.29 Calculated phase diagram in the system Na_2O-CaO-K_2O-FeO-MgO-Al_2O_3-SiO_2-H_2O-TiO_2 for a representative bulk composition of hydrated basalt (Manikyamba et al., 2015). The phase diagram has been constructed at 0.30 wt% CO_2 and 0.70 wt% of H_2O. The diagram has been constructed using the program Perple_X (see text for details). Note the position of the "melt-in" curve in the system. The two asterisks marked represent the P-T conditions from which the melt compositions have been recalculated (see text).

Figure 5.30 TAS diagram (after Middlemost, 1994) showing calculated melt compositions (a) at 900 °C, 8 kbar, and (b) 1000°C, 8 kbar. Note that the compositions plot in the quartz-monzonite and monzonite-monzodiorite fields at 900°C and 1000°C, respectively.

Figure 5.31 Chemical composition plots of trace element and REE measured from oscillatory-zoned zircon spots (a-h). Circles having different colours represent different samples. Different composition fields shown in the diagram are after Grimes et al. (2007, 2015). (a) U/Yb vs Hf plot. (b) U vs Nb plot. (c) Th vs Nb plot. (d) U/Yb vs Nb/Yb plot. (e) Ti vs Yb and (f) Ti vs Gd/Yb plot. (g) Multi-element trace and REE plot normalized to primitive mantle (Sun and McDonough, 1989). Colours used are same as used in (a-f). Note the prominent depletion of Ti and La and enrichment of U. Also note the flat to slightly enriched HREE plots. (h) Chondrite-normalized (after McDonough and Sun, 1995) REE pattern of the analyzed zircon showing prominent depletion in Pr and Eu and enrichment of Ce and Sm. Excepting a few samples (flat HREE pattern), most samples show enriched HREE pattern.

Figure 5.32 Log10 (U/Yb) vs log10 (Nb/Yb) plot of the analyzed oscillatory-zoned zircon. Symbols used are same as Fig. 5.31. Compositional fields and contours are after Grimes et al. (2015). Note that most of the sample's plot within the field of continental arc. The contours shown are for 50, 80, 90, and 95 % levels.

Figure 5.33-5.38 Photomicrographs of granites. (33) Symplectic intergrowth of biotite (Bt) + quartz (Qtz) on porphyroblastic garnet (Grt). (34) Large k-feldspar (Kfs) grain shows sub-grain formation and recrystallization. (35) Cuspate grain boundary and intergrowth between plagioclase (Pl) and quartz (Qtz), forming myrmekitic texture. (36) Micro-enclaves of aluminous granulite within granite containing mineral assemblage like sillimanite (Sil) + spinel + hemo-ilmenite grains. (37) Symmetric-asymmetric tails around garnet (Grt) within mylonitized granite. (38) Fine recrystallized matrix grains and quartz (Qtz) ribbons in mylonitized granite.

Figure 5.39-5.47 Geochemical plots of granites. (39) ASI vs A/NK plot after Frost et al., (2001) show peraluminous character. (40) SiO_2 vs FeO_t plot after Frost et al., (2001) show ferroan character. (41) MALI plot after Frost et al., (2001) shows broad range from calcic to alkali. (42) Total alkali vs silica (TAS) diagram plot after Middlemost (1994). (43) 1000*Ga/Al vs Zn plot after Whalen (1987). (44) Trace element plot after Sun and McDonough (1989), normalized to MORB values. Note that the plot shows enriched Rb, Th, K, Pb and Li and depleted Ba, Nb, Ta, Sr, P and Ti. (45) Rb vs Y + Nb plot after Pearce et al., (1984) show

overlapping characteristic between syn-collisional and within plate granite. (46) Nb/La vs La/Yb plot after Hollocher (2012) show arc signature. (47) REE) normalized to the primitive mantle (McDonough and Sun, 1995) show enriched LREE and depleted HREE trend.

Figure 5.48-5.49 Photomicrographs of monzosyenite (48) Magmatic layering with alternate biotite-rich and plagioclase (Pl) + K-feldspar (Kfs)-rich layers. (49) Clusters of zircons (Zrn) occur in association with ilmenite (Ilm), biotite (Bt) and plagioclase (Pl) (both under PPL).

Figure 6.1-6.13 Photomicrographs and BSE images of two pyroxene mafic granulite. (1) Magnetite (Mag_4) vein within plagioclase (Pl) in association with orthopyroxene (Opx) and clinopyroxene (Cpx). (2) ilmenite (Ilm_2) occurring along the margin of orthopyroxene (Opx) and antiperthitic K-feldspar (Kfs) within deformed plagioclase (Pl). (3) Thin film of K-feldspar (Kfs) along the margin of orthopyroxene (Opx). (4) Antiperthitic texture in plagioclase (Pl) where K-feldspar (Kfs) occur as patches. (5) Ilmenite (Ilm_2) partially engulfs magnetite (Mag_2). (6) Fine trellis hematite (Hem) intergrowth within ilmenite (Ilm_2). (7) Hematite (Hem) lamellae within ilmenite (Ilm_2), associated Mag_4 vein partially rims pyrrhotite (Po) and chalcopyrite (Cp). (8) Tripartite grain of magnetite (Mag_2), hemo-ilmenite (Ilm_2) and pyrite (Py) in association with plagioclase (Pl) and Opx. (9) Magnetite (Mag_1) inclusion within clinopyroxene (Cpx). Note the thin rim of quartz (Qtz) separating the two. (10) Tiny grains of orthopyroxene (Opx) along the margin of hornblende (Hbl). (11) Bipartite grain of magnetite (Mag_2) and ilmenite (Ilm_2). (12) Myrmekitic intergrowth of plagioclase (Pl) and quartz (Qtz) at the margin of perthite (Kfs). (13) Cuspate grain boundaries of K-feldspar (Kfs) and quartz (Qtz) in the matrix (shown in arrows).

Figure 6.14-6.16 Photomicrograph and BSE image of the garnet bearing mafic granulite. (14) Garnet (Grt) corona along with quartz (Qtz) around clinopyroxene (Cpx) and plagioclase (Pl). (15) Porphyroblastic clinopyroxene (Cpx) contains exsolved lamellae of orthopyroxene (Opx). (16) Porphyroblastic garnet (Grt) and Cpx grains along with Ilm_2 are stretched along the foliation.

Figure 6.17-6.26 BSE images showing oxide and sulphide phases of mafic granulite. (17) Pyrite (Py_1) in equilibrium contact with ilmenite (Ilm_2) and magnetite (Mag_2). (18) Relic pyrite (Py_1) within pyrrhotite (Po). Also note the tongue of chalcopyrite (Cp) in Po. (19) Pyrite (Py_2) marginally replaces pyrrhotite (Po). (20) Pyrrhotite (Po) is completely replaced by pyrite (Py_2) and magnetite (Mag_3). Note the relic of Po within Py_2. (21) Pyrrhotite (Po) and chalcopyrite (Cp) share a convolute mutual boundary within plagioclase (Pl). (22) Mantle of magnetite (Mag_3) on pyrite (Py_1). (23) Pyrite (Py_2) in contact with ilmenite (Ilm_2) is partially replaced by barite (Bar). Note the presence of thin veins containing Bar. (24) Discrete grain of calcite (Cc) and barite (Ba) in the matrix. (25) Thin barite (Bar) vein cutting through plagioclase (Pl). (26) Element X-ray map of Na (a) and Ca (b) in patchy antiperthite. The maps show Na-loss and concomitant Ca-gain of plagioclase.

Figure 6.27-6.28 (27) Plot of X_{Opx}^{Fe} vs. X_{Hem}^{Ilm} shows the correlation of the oxidation states between the oxide, sulphide and silicate phases of the studied mafic granulite samples. Samples represented by black symbols are dominated by Po–Py. The blue coloured filled symbol

represents samples dominated by Py–Mag with minor Po. (28) Plot of temperature vs. oxygen fugacities of the mafic granulite samples at 8 kbar. The positions of HM, NNO, CCO and QFM buffers are drawn for comparison and reference. Abbreviations used for assemblages: OMQ, orthopyroxene–magnetite–quartz; OHQ, orthopyroxene–hematite–quartz; AMQ, augite–magnetite–quartz; AHQ, augite–hematite–quartz.

Figure 7.1 CL images of representative zircon grains with 206Pb/238U dates in different samples. Spot numbers are also shown along with Th/U ratio (in parenthesis). The scale for each grain has a length of 100 μm. (a) Sample 17EG07. (b) Sample 17EG10. (c) Sample 17EG17. (d) Sample PH9A. (e) Sample 19EG06. (f) Sample PLB71B. (g) Sample PLB82A. (h) Sample PLB89A (i) Sample BLG3C.

Figure 7.2 Wetherill concordia plots for analyzed zircon grains from the studied charnockite samples. 206Pb/238U weighted average age for group of data showing oscillatory zoning is shown for each sample. (a) Sample 17EG07. (b) Sample 17EG10. (c) Sample 17EG17. (d) Sample PH9A, (e) Sample 19EG06. (f) Sample PLB71B. (g) SamplePLB82A. (h) Sample PLB89A (i) Sample BLG3C. For each sample, all data are plotted. Those used for group age calculations are shown as grey filled ellipses, while rest of the data are presented as open stippled ellipses.

Figure 8.1 Schematic diagram showing the reconstruction of the India-East Antarctica-Sri Lanka sector in the broad framework of the supercontinent East Gondwana (modified after Veevers, 2012). The representative P-T-t paths of the ca. 1000–900 Ma metamorphism from the EGP is from Bose et al. (2022) and Ganguly et al. (2018), while the same from the Rayner Province is from Harley (2003). Approximate locations of magmatic charnockite are shown in both the EGP (India) and the Rayner Province (East Antarctica). Abbreviations used: CGGC: Chotanagpur Gneissic Complex, SC: Singhbhum Craton, DC: Dharwar Craton, BC: Bastar Craton, MR: Mahanadi Rift, GR: Godavari Rift, SGT: Southern Granulite Terrain, WC: Wanni Complex, HC: Highland Complex, VC: Vijayan Complex, KP: Krishna Province, EGP: Eastern Ghats Province, LHC: Lutzow-Holm Complex, NC: Napier Complex, RP: Rayner Province, nPCM: Northern Prince Charles Mountains, FL: Fisher and Lambert terranes, RG: Ruker Group, VH: Vestfold Hills.

Figure 8.2 Cartoon diagram showing the tectonic development between India and East Antarctica during the time span of ca. 1380–900 Ma modified after Liu et al., (2014) and Bose et al. (2022). The cartoon shows phase-wise evolution of continental/magmatic arc in the sector and crystallization of charnockite magma in the Rayner-Eastern Ghats (R-EG) orogen. See text for details.